Japanese Journal of Applied Physics **54**, 033002 (2015) **REGULAR PAPER**
http://dx.doi.org/10.7567/JJAP.54.033002

X-ray photoelectron spectroscopic investigation on Fe geometrical sites of iron nitride thin films

Yin-Chih Lin[1†], Jhen-Yong Hong[1†], Chia-Nan Yen[1], Shi-Yuan Tong[2], Mean-Jue Tung[2], Hung-Wei Shiu[3], Chia-Hao Chen[3], and Minn-Tsong Lin[1,4*]

[1]*Department of Physics, National Taiwan University, Taipei 106, Taiwan*
[2]*Material and Chemical Engineering Laboratory, Industrial Technology Research Institute (ITRI), Hsinchu 300, Taiwan*
[3]*National Synchrotron Radiation Research Center (NSRRC), Hsinchu 300, Taiwan*
[4]*Institute of Atomic and Molecular Sciences, Academia Sinica, Taipei 106, Taiwan*
E-mail: mtlin@phys.ntu.edu.tw

Received October 15, 2014; accepted October 20, 2014; published online February 10, 2015

A partially ordered $Fe_{16}N_2$ thin film, which exhibits a higher saturation magnetization than a bcc-Fe thin film, was grown on a Au(001) texture on a GaAs(001) substrate for studies of crystalline structure, electronic structure, and magnetic properties. Fe $2p_{3/2}$ and $2p_{1/2}$ X-ray photoelectron spectroscopies (XPS) reveal the electronic hybridization between the Fe atoms and the adjacent N atoms, whereas a multipeak analysis suggests the charge-transfer-induced electronic rearrangement of electronic configuration in Fe(8h) and Fe(4e) geometrical sites. These results are consistent with the previous model and help explain the saturation magnetization enhancement in the α-FeN system.

1. Introduction

In contemporary magnetic industries, a material with high saturation magnetization, low coercive field, and resistance to oxidation is indispensable for fabricating devices and sensors. The bcc-Fe has a saturation magnetization of 1600 emu/cm^3, but is easily oxidized in air. The nitride state of iron is more chemically stable than its element state. α-FeN is considered a remarkable material for industrial application because of its high saturation magnetization[1–6] (1500 to 2350 emu/cm^3). α-FeN has two phases, α'-FeN (Fe_8N) and α''-FeN ($Fe_{16}N_2$), which have the same body-centered tetragonal (bct) structure ($a = b = 5.72$ Å, $c = 6.29$ Å[7]) and chemical ratio (Fe/N = 8[7]), but different order of Fe_6N octahedron. The Fe_6N octahedron in Fe_8N is randomly distributed, whereas that in $Fe_{16}N_2$ shows ordered distribution, as shown in Fig. 1(a). Depending on the geometrical rule and the distance of the nearest-neighboring N atom, the Fe in both Fe_8N and $Fe_{16}N_2$ could be classified into Fe(8h), Fe(4e), and Fe(4d) geometrical sites, as shown in Fig. 1(b). In previous years, Wang and coworker presented a reproducible and reliable FeN growth method[8,9] and discussed the effect of the N site.[10] The ordering of the Fe_6N octahedron cluster strongly affects the average saturation magnetization[10] (α'-FeN+α''-FeN) and plays a critical role in saturation magnetization enhancement. In addition to magnetic measurement by vibrating sample magnetometry (VSM), polarized neutron reflectometry (PNR) and X-ray magnetic circular dichroism (XMCD) were performed to directly carry out the in-depth saturation magnetization distribution[11,12] and element-specific magnetic moment.[8] Moreover, a theoretical model of "cluster(Fe_6N) and atom(Fe)" was presented to discuss the mechanism of saturation magnetization enhancement. The charge transfer between Fe and N in the Fe_6N cluster was predicted to play a critical role in the generation of a high saturation magnetization state, and probably to enhance the saturation magnetization.[13] However, the electronic structure of α-FeN is still unknown. In this study, X-ray photoelectron spectroscopy (XPS) was applied to probe the electronic structure of the FeN system and in turn clarify its impact on the magnetization properties of the α-FeN system.

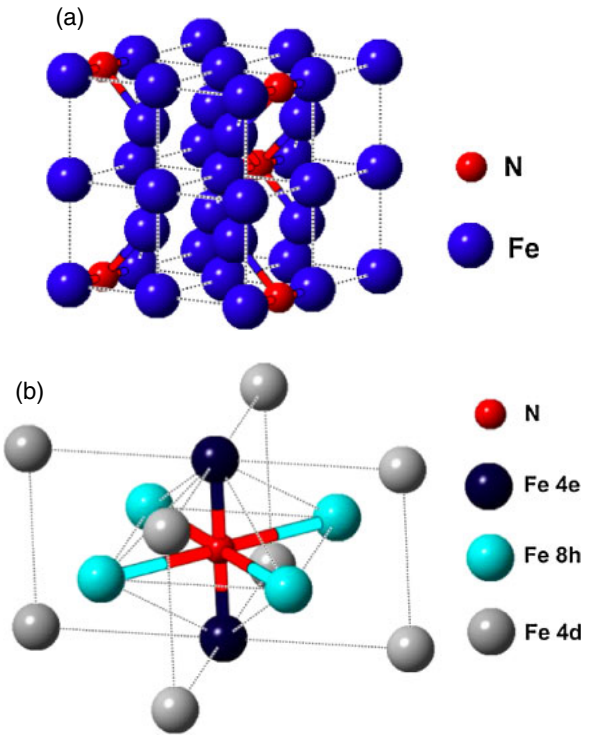

Fig. 1. (Color online) Crystalline structure of $Fe_{16}N_2$ with ordered N atom in the lattice. (b) Schematic diagram of Fe_6N octahedral cluster in the $Fe_{16}N_2$ structure. According to the geometrical rule, the Fe atom could be classified into Fe(4e), Fe(8h), and Fe(4d) geometrical sites.

2. Experimental procedure

The structure of our sample was designed with the following layer sequence: 2 nm Cu/FeN/buffered Au(001) texture/GaAs(001), in which the Cu thin film is used as a capping layer. Prior to the deposition, the wafer was cleaned and etched in the sequence of Piranha solution, hydrochloric acid (HCl), and deionized water. Au(001)-textured thin films were grown on a GaAs(001) substrate at 200 °C by thermal

†These authors contributed equally to this work.

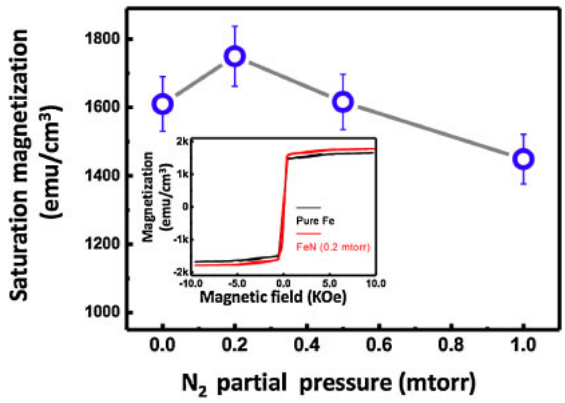

Fig. 2. (Color online) Saturation magnetization of Fe–N thin film as a function of N_2 partial pressure. The inset shows the magnetic hysteresis loops of the bcc-Fe sample (black curve) and FeN sample (red curve) fabricated under a N_2 partial pressure of 0.2 mTorr.

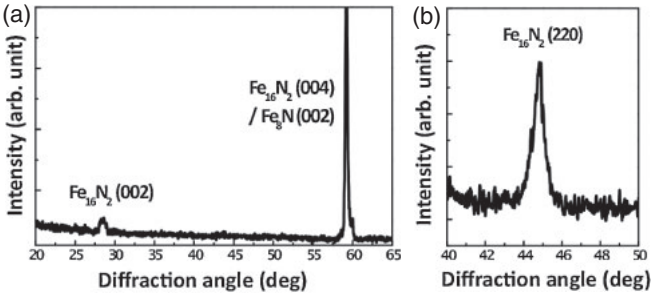

Fig. 3. GI-XRD of the FeN sample fabricated under a N_2 partial pressure of 0.2 mTorr with the scattering vectors along (a) the Au[011] direction, and (b) the Au[001] direction.

evaporation with a deposition rate of 0.2 Å/s,[14] whereas iron nitride thin films were deposited on the Au(001) texture at 100 °C in an Ar and N_2 mixture environment by DC sputtering (at the power of 150 W and a total pressure of 4 mTorr). The thickness was checked using atomic force microscopy (AFM; NPX 200) and a quartz crystal microbalance (QCM; Inficon XTM/2). The crystalline structure was characterized using grazing incidence X-ray diffraction (GI-XRD; TTRAX-3). The magnetic properties were measured using a vibrating sample magnetometer (VSM; Lakeshore 735) with the ultimate sensitivity of 10^{-6} emu. Prior to each measurement, the instrument was calibrated using a Ni sphere standard sample. To determine the saturation magnetization per unit volume (M_s), the magnetic moment was measured under a parallel magnetic field of 10 KOe. XPS with a high energy resolution of 0.05 eV was performed to examine the electronic structure at beamline 09A1 of the National Synchrotron Radiation Research Center (NSRRC) in Taiwan, followed by XPS data processing using XPSpeak software (version 4.1).[15]

3. Results and discussion

FeN thin film has various phases, such as γ-Fe_4N for face-centered tetragonal (fct) structure,[16,17] ϵ-Fe_3N for hexagonal close-packed (hcp) structure,[18,19] and α-FeN(α''-$Fe_{16}N_2$/α'-Fe_8N) for bodied-centered tetragonal (bct) structure.[20] During the reactive sputtering process, phase formation is strongly related to the amount of reactive gas (N_2) used and must be carefully examined. Figure 2 shows the saturation magnetization of the samples as a function of N_2 partial pressure ranging from 0 to 1.0 mTorr. The sample fabricated in a nitrogen-free environment exhibited a saturation magnetization of approximately 1600 emu/cm^3 (2.04 μ_B/Fe atom), which is the same as that of the standard bcc-Fe. The saturation magnetization becomes maximum at a N_2 partial pressure of 0.2 mTorr and decreases again as the N_2 partial pressure decreases. According to previous studies,[8,9] the generation of N-rich phases, such as those of γ-Fe_4N and ϵ-Fe_3N, might reduce saturation magnetization. As a result, the FeN sample fabricated under a N_2 partial pressure of 0.2 mTorr exhibited a saturation magnetization of 1750 emu/cm^3 (2.43 μ_B/Fe atom), which is clearly greater than that of bcc-Fe by over 10%. These results led to the fabrication of FeN with a higher saturation magnetization.

Among all FeN phases, only α''-FeN exhibits a higher saturation magnetization than a normal Fe thin film, whereas other phases, such as ϵ-Fe_3N and γ-Fe_4N, show lower saturation magnetization. This implies that the percentage of the ordered Fe_6N octahedron strongly affects the average saturation magnetization and needs to be examined. Figure 3 shows the GI-XRD spectra of the FeN sample fabricated under a N_2 partial pressure of 0.2 mTorr. When the scattering vector is aligned in the Au[011] direction, the peak at 28.4° represents the (002) plane of $Fe_{16}N_2$, and the peak at 59.2° reveals the combination of the (002) plane of Fe_8N and the (004) plane of $Fe_{16}N_2$. By aligning the scattering vector along the Au[001] direction, the peak at 45.0° shows the (220) plane of $Fe_{16}N_2$. The order degree of Fe_6N could be defined as[21,22]

$$D = \frac{[I_{\alpha''(002)}]^{obs}/[I_{\alpha''(004)} + I_{\alpha'(002)}]^{obs}}{[I_{\alpha''(002)}]^{cal}/[I_{\alpha''(004)}]^{cal}}, \quad (1)$$

where $[I_{\alpha''(002)}]^{obs}$ and $[I_{\alpha''(004)} + I_{\alpha'(002)}]^{obs}$ are the integrated intensities from the measurement, and $[I_{\alpha''(002)}]^{cal}$ and $[I_{\alpha''(002)}]^{cal}$ are the integrated intensities calculated for the $Fe_{16}N_2$ single crystal. The calculation indicates that the sample is a mixture of Fe_8N (random Fe_6N distribution) and $Fe_{16}N_2$ (ordered Fe_6N distribution) with $D = 0.296$. In contrast, the XRD spectra of the FeN sample fabricated under a N_2 partial pressure of 0.5 mTorr only show a peak at 59.2° (not shown here), which implies that the sample is only the Fe_8N phase ($D = 0$) and a very-high N_2 pressure may cause the random distribution of the Fe_6N cluster. These results suggest that the N_2 partial pressure strongly affects the formation of the $Fe_{16}N_2$ phase during fabrication.

To understand the enhanced saturation magnetization of α-FeN(α''-$Fe_{16}N_2$/α'-Fe_8N), a strong correlation[23] and the charge transfer via the existence of empty nitrogen orbitals[24] between the Fe atom and the N atom were proposed. However, in the model of "cluster(Fe_6N) and atom(Fe)", only the ordered Fe_6N octahedral cluster contributes to the generation of a high magnetic state.[13] The ordered Fe_6N in $Fe_{16}N_2$ has strong Coulumb interaction, which results in the charge difference between interior and exterior parts of the Fe_6N octahedral cluster.[13] The N atom functions as a medium that transfers the charges between adjacent Fe(8h) and Fe(4e) atoms. The high magnetic state of 4 μ_B per Fe atom is induced in Fe(4e) and Fe(8h) geometrical sites.[13]

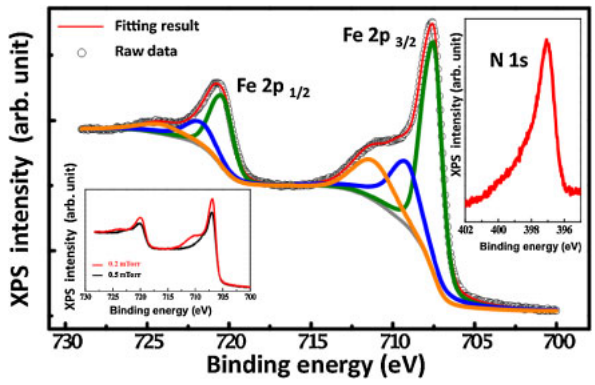

Fig. 4. (Color online) Fe $2p_{3/2}$ and $2p_{1/2}$ XPS curves of FeN sample fabricated under a N_2 partial pressure of 0.2 mTorr. The open circles and red curve represent the original data and the best fitted result, respectively. The insets show the N 1s spectrum of the FeN sample fabricated under 0.2 mTorr and the normalized Fe 2p spectrum of the FeN sample fabricated under 0.2 (red curve) and 0.5 (black curve) mTorr. (Photon energies are 900 eV for the Fe spectrum, and 620 eV for the N spectrum.)

Table I. Fitting result of Fe 2p spectrum by the analysis of XPSpeak software (version 4.1).

	Binding energy (eV)	FWHM (eV)	Intensity (%)	Source
Fe $2p_{3/2}$	707.0	1.1	53.7	Fe in Fe_8N, Fe(4d) in $Fe_{16}N_2$
	708.5	1.8	30.9	Fe(8h) in $Fe_{16}N_2$
	710.5	2.7	15.4	Fe(4e) in $Fe_{16}N_2$
Fe $2p_{1/2}$	719.8	1.2	55.4	Fe in Fe_8N, Fe(4d) in $Fe_{16}N_2$
	721.1	1.8	29.5	Fe(8h) in $Fe_{16}N_2$
	723.5	2.6	15.1	Fe(4e) in $Fe_{16}N_2$

However, in the disordered Fe_6N octahedron, the charge difference between interior and exterior parts disappears because of random distribution.[13] Therefore, the Fe sites in Fe_8N maintain the normal magnetic state of 2 μ_B per Fe atom, which is the same as in the case of the pure Fe thin film. The charge transfer in ordered $Fe_{16}N_2$ was predicted using this model. To discover the supporting evidence for charge transfers by observing the electronic structures, high-energy resolution XPS was used to probe the details of the electronic structure.

Prior to the measurement, the samples were sputtered using 2 kV Ar ions until the surface signal of Cu disappeared entirely and a Au standard sample was used for energy calibration. The crystalline structure of the sample was checked again by using XRD, which excludes the possibility of structure damage during the Ar-plasma process. Figure 4 shows the Fe 2p and N 1s spectra of the sample fabricated under a N_2 partial pressure of 0.2 mTorr. The Fe 2p spectrum resembles the main peak and the neighboring shoulder peak. By using the multi-peak curve fitting process, the Fe $2p_{3/2}$ spectrum can be decomposed into three contributions: (1) 707.0, (2) 708.5, and (3) 710.5 eV. The main peak at a binding energy (BE) of 707.0 eV represents the Fe in Fe_8N and Fe(4d) geometrical site in $Fe_{16}N_2$, which is located at the same BE as standard Fe (707.0 eV).[25] The remaining peaks at BEs of 708.5 and 710.5 eV, which are attributed to the geometrical sites of Fe(8h) and Fe(4e), exhibit an energy shift toward the higher binding energy. The energy shift of the Fe(4e) peak is larger than that of the Fe(8h) peak because the distance between the Fe(4e) atom and N atom is much smaller than that in the case of Fe(8h). Quantitatively, the intensities of Fe(8h) and Fe(4e) are estimated as 30 and 15%, respectively, as listed in Table I. Taking into account that the intensity of Fe(4d) in $Fe_{16}N_2$ is 15% according to the proportion[10] of Fe(4d) : Fe(8h) : Fe(4e) = 1 : 2 : 1, $Fe_{16}N_2$ is estimated to be approximately 60% in the sample, which is larger than the estimation ($D = 29.6\%$) from the XRD result. Because the scattering coefficients of $I_{\alpha''(004)}$ and $I_{\alpha'(002)}$ are different, the composition of $Fe_{16}N_2$ could not be deduced directly from the D value. This behavior is not only shown in the Fe $2p_{3/2}$ spectrum but also in the Fe $2p_{1/2}$ spectrum. The inset in Fig. 4 shows the clearly different features at the shoulder parts in the Fe 2p spectrum of the FeN samples, which were fabricated under N_2 pressures of 0.2 (red curve) and 0.5 (black curve) mTorr. Moreover, the peak in the N 1s spectrum at a BE of 397.0 eV exhibits a shift toward the lower energy as compared with the single-atom state (409.9 eV)[26] and the adsorption state (403.9 eV).[27] The energy shift in the XPS spectrum implies that the electronic hybridization may be caused by the rearrangement of electronic configuration in the Fe and N core levels, which proves the existence of charge transfers in the Fe and N atoms in Fe_6N octahedral clusters.

4. Summary

In summary, the partially ordered $Fe_{16}N_2$ thin film exhibits a higher magnetization than the bcc-Fe thin film sample. Fe 2p and N 1s spectra, along with the multipeak analysis, indicate the electronic hybridization between the N atoms and the adjacent Fe atoms in $Fe_{16}N_2$, which in turn supports the charge transfer phenomenon in the proposed cluster(Fe_6N) and atom(Fe) model. The study suggests that understanding of the electronic interaction between Fe and N atoms could help in the investigation of the saturation magnetization enhancement in the partially ordered $Fe_{16}N_2$ system.

Acknowledgments

The work was supported by the Industrial Technology Research Institute (ITRI) of Taiwan under the FY101-102 program and the National Science Council (NSC) of Taiwan under Grant Nos. 101-2112-M-002-024-MY3 and 102-2120-M-002-005.

1) T. K. Kim and M. Takahashi, Appl. Phys. Lett. **20**, 492 (1972).
2) Y. Sugita, K. Mitsuoka, M. Komuro, H. Hoshiya, Y. Kozono, and M. Hanazono, J. Appl. Phys. **70**, 5977 (1991).
3) D. C. Sun, E. Y. Jiang, M. B. Tian, C. Lin, and X. X. Zhang, J. Appl. Phys. **79**, 5440 (1996).
4) C. Ortiz, G. Dumpich, and A. H. Morrish, Appl. Phys. Lett. **65**, 2737 (1994).
5) M. Takahashi, H. Shoji, H. Takahashi, H. Nashi, T. Wakiyamam, M. Doi, and M. Matsui, J. Appl. Phys. **76**, 6642 (1994).
6) K. Nakajima and S. Okamoto, Appl. Phys. Lett. **54**, 2536 (1989).
7) K. H. Jack, Proc. R. Soc. London, Ser. A **208**, 200 (1951).
8) J. P. Wang, N. Ji, X. Liu, Y. Xu, C. Sanchez-Hanke, Y. Wu, F. M. F. de Groot, L. F. Allard, and E. Lara-Curzio, IEEE Trans. Magn. **48**, 1710 (2012).

9) N. Ji, Y. Wu, and J. P. Wang, J. Appl. Phys. **109**, 07B767 (2011).
10) N. Ji, L. F. Allard, E. Lara-Curzio, and J. P. Wang, Appl. Phys. Lett. **98**, 092506 (2011).
11) N. Ji, V. Lauter, H. Ambaye, and J.-P. Wang, SPIN **2**, 1250004 (2012).
12) N. Ji, V. Lauter, X. Zhang, H. Ambaye, and J. P. Wang, Appl. Phys. Lett. **102**, 072411 (2013).
13) N. Ji, X. Liu, and J. P. Wang, New J. Phys. **12**, 063032 (2010).
14) D. Y. Noh, Y. Hwu, H. K. Kim, and M. Hong, Phys. Rev. B **51**, 4441 (1995).
15) Web [http://www.uksaf.org/software.html].
16) K. Ito, G. H. Lee, K. Harada, M. Suzuno, T. Suemasu, Y. Takeda, Y. Saitoh, M. Ye, A. Kimura, and H. Akinaga, Appl. Phys. Lett. **98**, 102507 (2011).
17) B. C. Frazer, Phys. Rev. **112**, 751 (1958).
18) A. Leineweber, H. Jacobs, F. Huning, H. Lueken, H. Schilder, and W. Kockelmann, J. Alloys Compd. **288**, 79 (1999).
19) K. H. Eickel and W. Pitsch, Phys. Status Solidi **39**, 121 (1970).
20) N. Ji, M. S. Osofsky, V. Lauter, L. F. Allard, X. Li, K. L. Jensen, H. Ambaye, E. Lara-Curzio, and J. P. Wang, Phys. Rev. B **84**, 245310 (2011).
21) S. Okamoto, O. Kitakami, and Y. Shimada, J. Magn. Magn. Mater. **208**, 102 (2000).
22) S. Okamoto, O. Kitakami, and Y. Shimada, J. Appl. Phys. **79**, 5250 (1996).
23) W. Y. Lai, Q. Q. Zheng, and W. Y. Hu, J. Phys.: Condens. Matter **6**, L259 (1994).
24) A. Sakuma, J. Appl. Phys. **79**, 5570 (1996).
25) C. D. Wager, M. W. Riggs, L. E. Davis, J. F. Moulder, and G. E. Mullenberg, *Handbook of X-ray Photoelectron Spectroscopy* (Perkin-Elmer, Eden Prairie, MN, 1979) Chap. 1, p. 80.
26) *Photoemission in Solids I: General Principles*, ed. M. Cardona and L. Ley (Springer, Berlin, 1978) Chap. 6, p. 266.
27) H. Tillborg, A. Nilsson, B. Hernnas, N. Martensson, and R. E. Palmer, Surf. Sci. **295**, 1 (1993).